Renewable Energy 202 (2023) 1032–1045

Contents lists available at ScienceDirect

Renewable Energy

journal homepage: www.elsevier.com/locate/renene

Structural instrumentation and monitoring of the Block Island Offshore Wind Farm

Eric M. Hines [a,*], Christopher D.P. Baxter [b], David Ciochetto [c], Mingming Song [a,f], Per Sparrevik [d], Henrik J. Meland [d], James M. Strout [d], Aaron Bradshaw [b], Sau-Lon Hu [b], Jorge R. Basurto [e], Babak Moaveni [a]

[a] Dept. of Civil and Environmental Engineering, Tufts University, Medford, MA, USA
[b] Depts. of Ocean/Civil and Environmental Engineering, University of Rhode Island, Kingston, RI, USA
[c] Rhode Island Coastal Resources Management Council, RI, USA
[d] Norwegian Geotechnical Institute, Oslo, Norway
[e] Ørsted, Kraftværksvej 53 - Skærbæk, 7000, Fredericia, Denmark
[f] Department of Bridge Engineering, Tongji University, Shanghai, China

ARTICLE INFO

Keywords:
Structural health monitoring
Offshore wind turbines
Block Island Wind Farm
Digital twins
Continuous monitoring system
Instrumentation design

ABSTRACT

This work presents the design and installation of a continuous monitoring system for one of the offshore wind turbines in the Block Island Wind Farm, which is located 6.1 km off the coast of Block Island in Rhode Island, USA. The instrumentation plan includes wired and wireless accelerometers, strain gauges, and inclinometers. Considerations for the instrumentation design are discussed, including the type, number and location of sensors, as well as some of the challenges in the installation of sensors. The process of transferring data, samples of collected data, automated system identification and some preliminary results are presented.

1. Introduction

Wind energy is now the largest source of renewable electricity in the US, supplying 10.6% of net Summer electric capacity in 2020 [1]. State targets for offshore wind energy have reached over 40 GW [2]. Meanwhile, the size and complexity of offshore wind turbines (OWT) have also grown rapidly to sizes of 15+ MW [3].

OWTs are exposed to harsh weather and marine environmental conditions. This results in continuous cyclic loading, including wind and wave loads, which leads to highly variable operational conditions and intense mechanical stress. The operation and maintenance (O&M) cost can consist of 10–20% of the total cost of energy for a wind project, and this number can go up to 35% at the end of life [4]. Due to maintenance requirement and mechanical failures, operational unavailability of wind turbines can reach 3% of its lifetime, which significantly reduces their efficiency and increases cost of energy. As the offshore wind industry continues to grow exponentially, it is critical to increase the reliability and reduce the O&M cost for these machines that are difficult and costly to reach and maintain. Maintenance approaches in the wind industry can be generally classified into three categories: corrective maintenance (run to failure), preventive maintenance (time-based) and predictive maintenance (condition-based) [4]. In the corrective maintenance strategy, expensive repair cost is required and long downtimes will be experienced due to mechanical faults and unexpected failures. For preventive maintenance, mechanical components are replaced in a time-based manner without consulting their actual conditions, which will prevent potential failures but with the expense of high prevention cost as many replaced parts are still in good condition and useable. The condition-based predictive maintenance approach combines the benefits of the preventive and corrective maintenance because it can be developed to predict and detect mechanical faults and result in replacement of parts only when necessary. Therefore, condition monitoring of offshore wind turbines instituted during the early days of the U.S. offshore wind industry can provide substantial financial benefits and reduce the levelized cost of energy over the long term [5–8].

The development of affordable long-term structural monitoring campaigns for offshore wind turbines in U.S. waters will allow owners and regulators not only to track the wear and tear on these valuable assets over time, but also to study signals provided by these assets prior to ‘faults’ such as structural damage or mechanical and electrical

* Corresponding author. Department of Civil and Environmental Engineering, Tufts University, 200 College Ave., Medford, MA, 02155, USA.
E-mail address: eric.hines@tufts.edu (E.M. Hines).

https://doi.org/10.1016/j.renene.2022.11.115
Received 7 June 2022; Received in revised form 17 November 2022; Accepted 26 November 2022
Available online 30 November 2022

Fig. 1. BIWF geographic location, turbine B2, and elevation view of the five OWTs (photo credit: Eric Thayer/Bloomberg).

malfunction. The development of effective fault diagnosis methods requires the establishment of monitoring systems prior to the occurrence of a fault. With such systems in place, pre-fault signals can provide a basis for learning and improvement to the monitoring system's predictive capacity.

1.1. Literature survey

As the benefit of condition monitoring of wind turbines has been acknowledged by the wind industry, numerous condition monitoring systems have been implemented in recent years [9]. Devriendt et al., 2014 installed a structural health monitoring system on an offshore wind turbine at Belwind wind farm in the Belgian North Sea and performed automated operational modal analysis over two weeks when the turbine was parked or idling [10]. Oliveira et al., 2016 implemented a monitoring system at a 2 MW onshore wind turbine at north of Portugal and automatically extracted modal parameters of the wind turbine during a period of 1 year [11]. In addition, several condition monitoring platforms have been created for the purpose of research and education, for instance, the 7 MW Levenmouth Demonstration Turbine [12], the twelve 5 MW turbines at Alpha Ventus [11], the Clipper Liberty C96 2.5 MW wind turbine [13], and a series of Research Platforms in the North and Baltic Seas, known as FINO1, FINO2, and FINO3 [14,15].

In many condition monitoring systems, an automated system identification approach is often employed to extract modal parameters of the wind turbine, which are then used to assess the structural conditions and detect potential damage. Modal parameters have been used extensively as informative data features in the field of structural health monitoring (SHM). Model updating is one of the most popular methods in SHM and is a process of fusing measurements and a numerical model to estimate uncertain model parameters, improve model predictions, and identify structural damage. Model updating can be performed in a traditionally deterministic manner when an objective function which consists of misfit between model-predictions and measurements is minimized [16–23], or in a probabilistic way where Bayesian inference is often employed to infer a posterior distribution of uncertain model parameters [24–32]. In addition, unknown input loads (e.g., wind and wave loads) on the wind turbines can also be estimated using the measured data by the condition monitoring system [15,33–41]. The input information is valuable for structural design or assessment of structural condition in similar environment.

1.2. Contributions

This paper presents the design and installation of a continuous monitoring system for one of the offshore wind turbines (B2) in the Block Island Wind Farm (BIWF), in Rhode Island, USA. Commissioned in December 2016 and consisting of five 6 MW GE Halide 150 turbines, the BIWF is the first commercial U.S. offshore wind farm. Originally designed and constructed by Deepwater Wind with U.S. manufactured jacket foundations, BIWF is currently owned and operated by the Danish offshore wind developer Ørsted, who acquired Deepwater Wind in October 2018 [42]. BIWF is located approximately 3 miles southeast of Block Island in Rhode Island state waters and was permitted on January 20, 2015 under the authority of the Rhode Island Coastal Resources Management Council (CRMC) [43]. The structural monitoring project discussed in this paper, known as the Block Island Structural Monitoring Joint Project (BISM-JP), was approved under a research stipulation of Section O. of the BIWF letter of Assent [43]. The project was funded by the U.S. Bureau of Safety and Environmental Enforcement (BSEE), and has been overseen jointly by CRMC, BSEE, and the U.S. Bureau of Ocean Energy Management (BOEM). These instruments and data acquisition system have provided continuous real-time data since their 2021 installation for the purpose of establishing benchmark data sets describing offshore wind structural performance in coastal U.S. waters. This data is intended to help guide planning and regulation of future commercial scale U.S. offshore wind farms. This paper describes the instrumentation, data acquisition and basic modal behavior of Turbine B2 on this first-of-a-kind U.S. OWT structural monitoring campaign.

Although some monitoring systems of wind turbines have been installed around the world and corresponding modal analyses have been performed, this study presents the monitoring campaign of the first commercial offshore wind farm in the U.S. which has the special jacket-type substructure compared to common monopiles. The monitoring system has been streaming data since the installation and has lasted over a year, which provides an experimental database and benchmark modal properties under varying environmental and operational conditions for future assessment and prognosis of OWTs in U.S. waters. The BIWF and Turbine B2 are shown in Fig. 1. Turbine B2 stands in 27.75 m of water on a U.S. manufactured four-legged jacket structure anchored to the ocean floor with pipe piles driven through the jacket legs into sand and stiff clay to embedment depths of 51.8–54.4 m.

1.3. Organization of the paper

The paper is organized as follows: Section 2 presents the design and

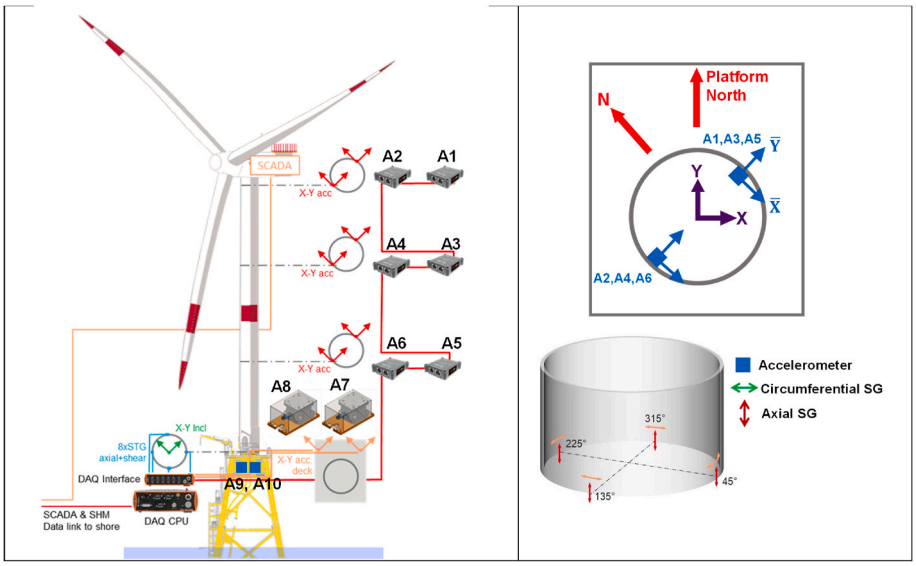

Fig. 2. Elevation (a) and top view (b) of instrumentation plan.

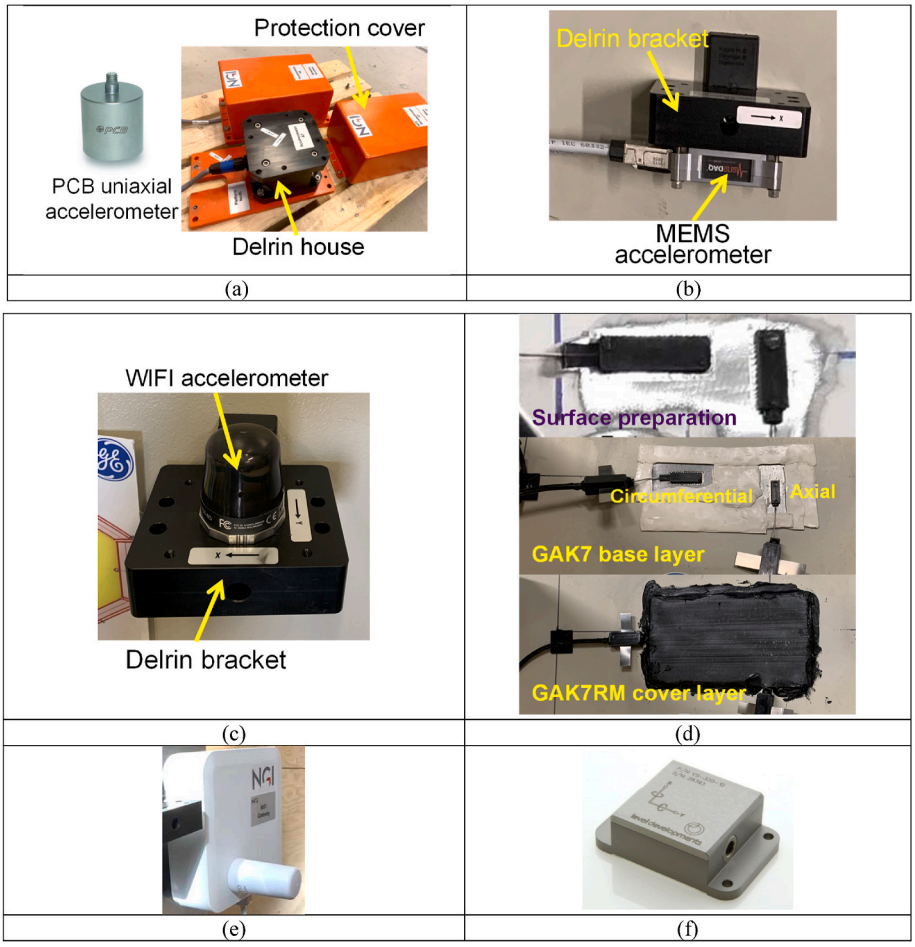

Fig. 3. (a) Retrofitted biaxial accelerometer using two PCB uniaxial accelerometers; (b) MEMS triaxial accelerometer mounted on Delrin bracket with magnet fixture; (c) Wireless accelerometer mounted on Delrin bracket; (d) Installation process of SGs; (e) Gateway transceiver for wireless accelerometers; (f) Biaxial inclinometer.

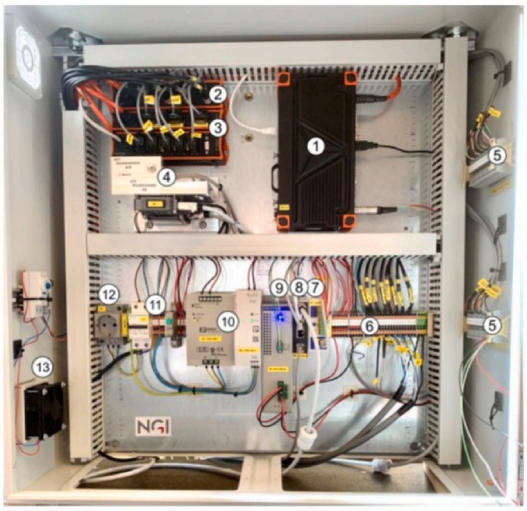

Fig. 4. DAQ box.

instrumentation of the monitoring system; Section 3 presents samples of measurements and preliminary modal parameter results using the proposed automated system identification approach; Finally, Section 4 summarizes the paper.

2. Continuous monitoring system

2.1. Sensor layout and locations

The sensor locations were designed based on the following considerations:

1. Sensors must be installed without the need for a rope-team or divers, so suitable locations only include the deck platform and the tower;
2. Sensor locations should be at existing platform levels. The existing platforms along the tower provides accessibility to both sides of the tower;
3. Wired sensors should be close to exiting cable trays;
4. Sensors should be able to measure the fore-after, side-side and torsional motions of the structure; and
5. Strain measurements are required in addition to the acceleration data in order to be able to estimate the fatigue life of the structure.

The resulting sensors of the continuous monitoring system currently consist of 9 wired accelerometers, 4 wireless accelerometers, 8 strain gauges (SG), and 1 inclinometer. The accelerometers, the inclinometer and the data acquisition system (DAQ) were installed in April 2021, with final approval on April 18, 2021. The SGs were installed on October 24, 2021. The monitoring system, including sensors, cables, and data acquisition system, were designed and provided by the Norwegian Geotechnical Institute (NGI, Inc.). The instrumentation plan of wired accelerometers and data acquisition system are shown in Fig. 2.

The wired accelerometers are named as ‘A1’ to ‘A10’. A7, A8 and A10 are retrofitted biaxial accelerometers, and the others are MEMS triaxial ones. A1 – A6 accelerometers were placed along the height of the tower at three different levels: A1 and A2 were mounted on the opposite inner surface of the tower at 76.9 m above the deck platform; similarly, A3 and A4 are located at 52.4 m, and A5 and A6 are located at 27.9 m. This layout was intended to measure the torsional motion of the turbine structure. A7 was mounted on the northeast corner of the platform (relative to platform north). A8 was not mounted due to cabling constraints encountered on site. A9 and A10 were placed inside the DAQ cabinet for comparative testing, which can also be used as spares to external sensors.

The measurement directions of the accelerometers ($\overline{X}$ and $\overline{Y}$) are rotated 45° clockwise from the structural coordinate system (X and Y). Four wireless triaxial accelerometers were placed at four elevations along the tower. The 4 axial SGs and 4 circumferential SGs were paired one to one and mounted at 4 symmetric points 0.7 m above the deck platform on the inner surface of the tower, as shown in Fig. 2(b). The 9 wired accelerometers and the inclinometer are working properly and providing high-quality measurements continuously since April 18, 2021, and additional strain data are collected since October 24, 2021. The monitoring system has a sampling frequency of 50 Hz and stores every 10 min measurements into a series of data sets.

2.2. Choice of sensors

At the top of the tower and at approximately the tower third points, accelerometers A1-A6 were designed as triaxial MonoDAQ-E-gMeter fully integrated low-noise 3D MEMS accelerometers with EtherCAT interface. The small and lightweight MEMS accelerometers were mounted underneath a Delrin bracket with magnet fixture for easy attachment to the vertical steel walls inside the tower (Fig. 3(b)). For testing and additional dynamic data acquisition, 4 wireless triaxial accelerometers (Fig. 3(c)) with a gateway transceiver were mounted inside the tower wall by a magnetic footing. The wireless accelerometers are Lord MicroStrain IP67 units which are small and lightweight (150 g). The wireless nodes are battery driven with a capacity of at least 1-month continuous recording. Each wireless accelerometer unit communicates directly to the gateway transceiver (Fig. 3(e)) with magnetic mount. The gateway had been modified with an external omni directional (360°) antenna, which was mounted horizontally for best transmission of the vertical direction inside the tower. At the base of the tower and on the platform, very low accelerations were expected and therefore higher sensitivity accelerometers were deployed at A7-A10, consisting of 2 PCB 393B04 ICP accelerometers in perpendicular directions and mounted inside a waterproof Delrin enclosure to work as a biaxial accelerometer (shown in Fig. 3(a)). Two of these biaxial accelerometers were built for measurement on the deck. The biaxial accelerometer enclosure was mounted on the deck by means of a doubler plate and protected against impact by a painted steel cover (Fig. 3(a)).

The SGs are full bridge and temperature compensated spot weldable axial (HBWF-35-125-6-99UP-SS) and circumferential SGs (HBWS-35-125-6-99UP-SS-FB) provided by HPI, as shown in Fig. 3(d). The 4 axial SGs and 4 circumferential SGs are paired one to one and mounted together on the inner surface of the tower. To mount the SG, grinding and polishing were required to remove the steel coating, and then the

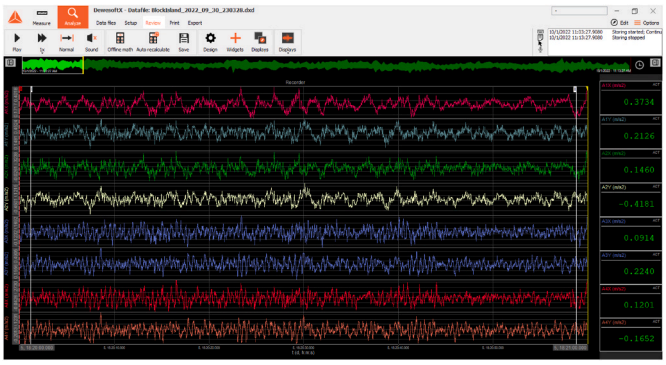

Fig. 5. Data streaming using DEWEsoft-X3.

surface was cleaned with solvent. Then an axial SG is attached to the surface vertically, and the circumferential SG is placed horizontally (Fig. 3(d)). After the completion of SG installation, GAK7 base layer was applied around the SG and cover the grinded surface. Finally, GAK7RM cover layer was used to cover the base layer, and GAK1100 was injected under the rubber flap around the edge of cover plate. These processes are shown in Fig. 3(d). The inclinometer is a temperature compensated biaxial MEMS inclinometer, which was mounted inside the DAQ cabinet, as shown in Fig. 3(f).

2.3. Data acquisition system

The data acquisition system (DAQ) was located inside the transition piece. A fiber optic link was used to connect the DAQ to the substation in Block Island. The recorded and filtered data was streamed over this fiber optic link without any need of data reduction. The CPU in the DAQ can be operated remotely using the TeamViewer software via the fiber optic link and internet access. The main frequency band of interest for dynamic measurements at Block Island is 0.1–10 Hz. To avoid aliasing effects, data is sampled at 50 Hz and low pass filtered by the DAQ CPU with a 10 Hz 6th order Butterworth filter. To achieve the required data synchronization for modal shape analyses, EtherCAT LAN based streaming was used and provided millisecond synchronization between the sensor channels. The EtherCAT streaming accelerometers (A1 - A6) and other type of sensors (retrofitted biaxial accelerometers, inclinometer and 8 SGs) were hooked up directly or via interface modules to the EtherCAT line for synchronized logging by the DAQ CPU. Each sensor or data acquisition unit can be distributed along the EtherCAT LAN, and the wired accelerometers are powered over Ethernet. The system architecture allows for flexible configuration and connectivity. Each sensor and interface unit are automatically recognized and configured by the small and ruggedized (IP67) DAQ CPU. The CPU sampling can be synchronized to external systems by GPS time and operated remotely via the fiber optic link and internet access.

The main components of the DAQ are shown in Fig. 4. DEWESoft-X3 software is installed on the DAQ CPU for system configuration, real-time analysis/checks and data export/storage. DEWESoft-X3 includes hundreds of prepared calculation algorithms, display and analysis functions that do not require any programming from the user, examples of processing features include: fast Fourier transform, statistics calculation, IIR and FIR filtering, event-triggered data storage, GPS timing, integration and derivation, and data exportation to other platforms, for example, Excel or Matlab. When a DAQ device is connected to the computer, DEWESoft-X3 will recognize it automatically and display the list of available analogue channels. A screenshot of the data streaming using Dewesoft-X3 is shown in Fig. 5. The data was stored in proprietary binary file format (.d7d) that can be exported to other formats. Please note that these embedded functions and algorithms in DEWESoft-X3 are only used to investigate the data quality and check the status of the monitoring system, the continuous streaming data are directly saved fully to preserve the original measurements of the OWT. In Section 3.2, the raw measurements are preprocessed by removing spikes, filtering noise and down-sampling to improve system identification accuracy, but these processes only happen in Matlab for system identification, and the original measurements remain untouched. A Box cloud storage are allocated enough space to save the huge amount of raw data. Every 10 min of data from all sensors is saved into a binary data file which is approximately 5.6 MB. This means that all the data from one year of monitoring is less than 300 GB.

2.4. Data transfer and storage

The streamed data on B2 OWT can be stored locally in the DAQ CPU which was equipped with a removable 250 GB SATA solid state drive. In addition, the data was also transferred directly to the substation in Block Island through fiber optic cable. The transferred data were then uploaded to a Box cloud storage by the laptop at the substation through a cellular hotspot. The data transfer process is illustrated in Fig. 6.

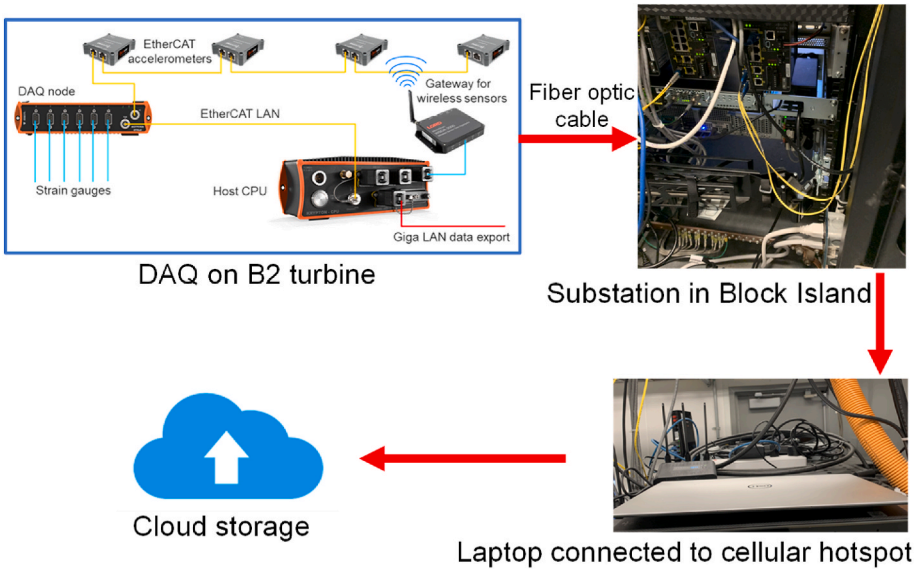

Fig. 6. Data transfer process.

3. Preliminary system identification results

3.1. Sample of collected data

Samples of acceleration, strain and inclination angle time histories are shown in Figs. 7, 9 and 10, respectively. Accelerometers A9 and A10 are mounted inside the DAQ cabinet, and the comparison of their acceleration time histories are shown in Fig. 8. It is seen that their measurements agree with each other well. To quantify the difference between measurements of A9 and A10, relative root-mean-square error (RRMSE) is evaluated, which is defined as $\mathrm{RMS}(\mathrm{A9}-\mathrm{A10})/\ \mathrm{RMS}(\mathrm{A9})$ where RMS stands for root-mean-square. The RRMSEs are 0.15 for X direction and 0.52 for Y direction. The Fourier amplitude spectra (FAS) of acceleration, strain and inclination are plotted in Figs. 11–13. From Fig. 11, it is observed that the most significant peak is located at around 0.3 Hz which represents the first bending modes in fore-aft (FA) and side-side (SS) directions of the turbine. The 3P and 6P peaks are also evident which are caused by the rotor rotation and have frequencies of 3 times (3P) and 6 times (6P) of the revolution frequency of the rotor. Based on the specification of the wind turbine, the rotor has a speed range of 4–11.5 rpm, which represents a 1P frequency range of 0.067–0.192 Hz. Therefore, the 3P and 6P have ranges of 0.2–0.575 Hz, and 0.4–1.15 Hz, respectively.

It is worth noting that 1P, unlike 3P and 6P, is hardly noticeable in

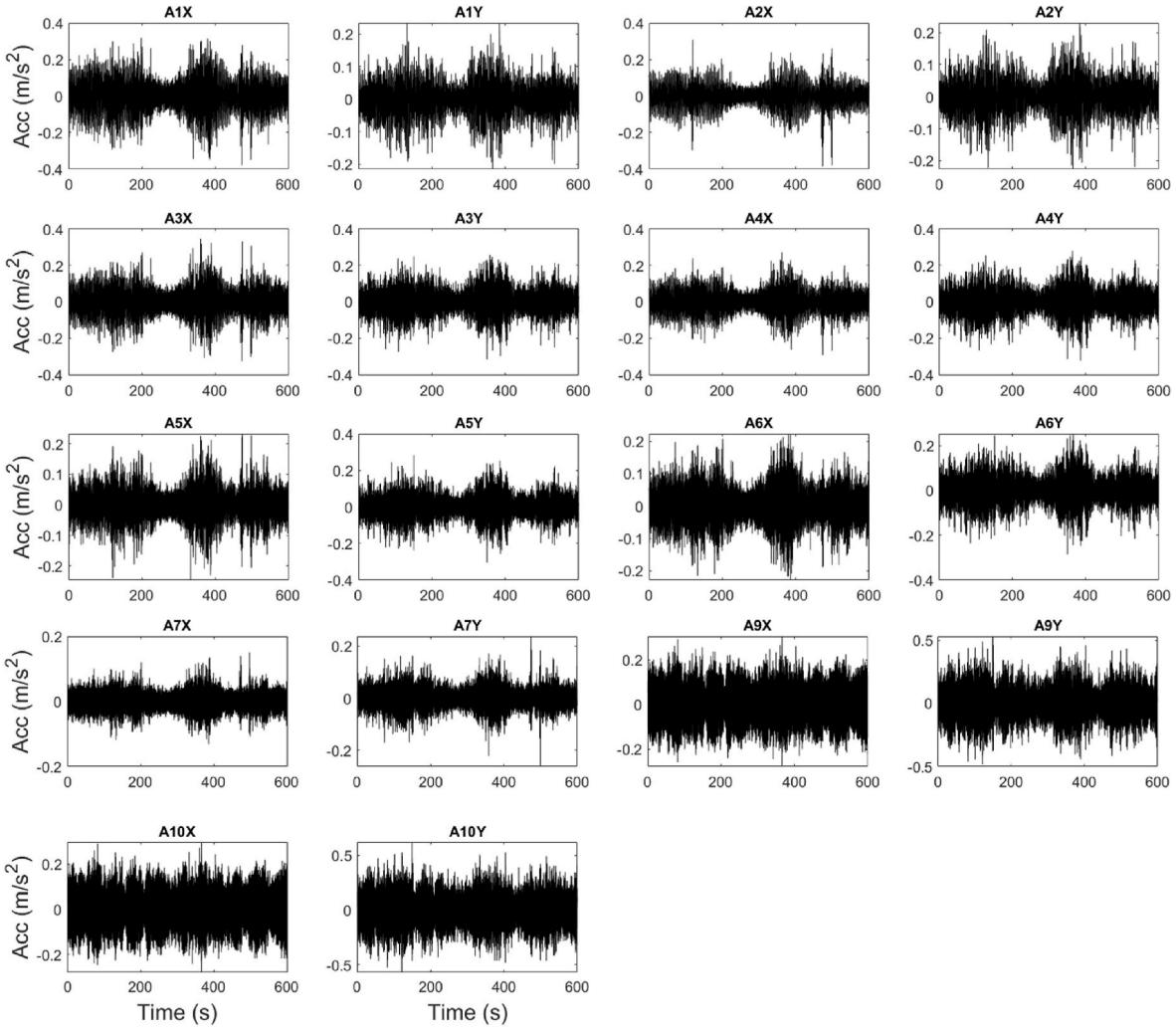

Fig. 7. Sample of acceleration time histories at 9:17 on April 22.

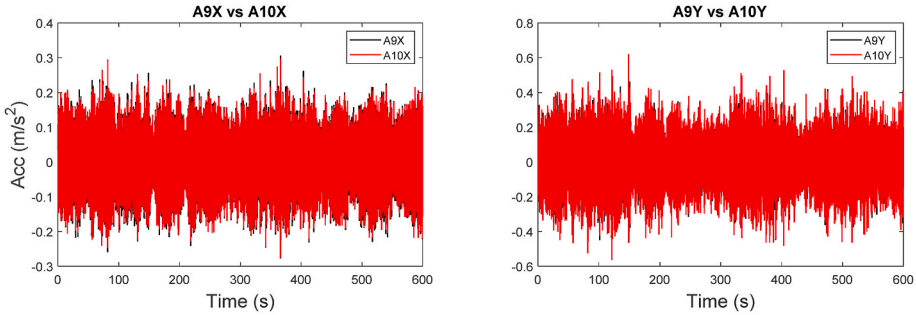

Fig. 8. Comparison of acceleration time histories from A9 and A10.

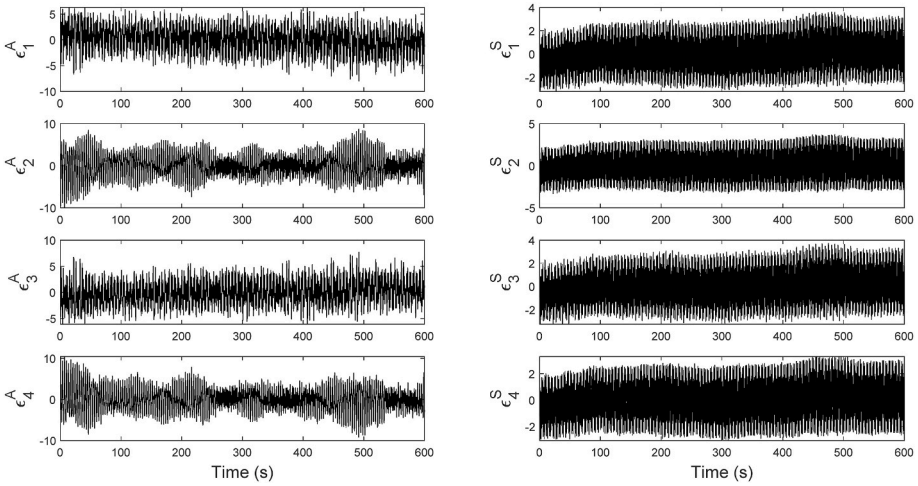

Fig. 9. Sample of strain time histories at 16:03 on October 25 (unit: $\mu\varepsilon$).

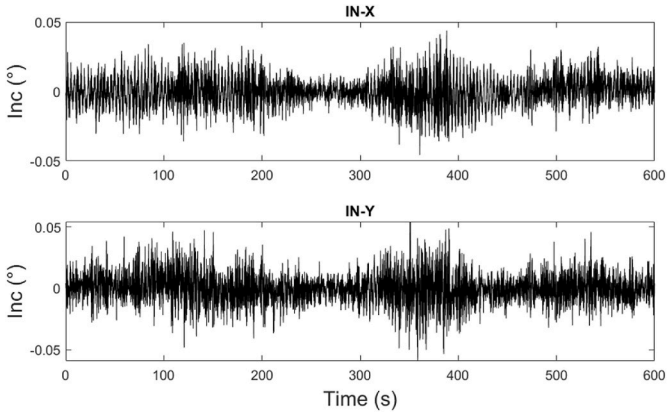

Fig. 10. Sample of inclination time histories at 9:17 on April 22.

the FAS plots of acceleration measurements (Fig. 11) but is evident in the FAS of strain data (Fig. 12). The FAS of strain data show evident peaks for 1P, 3P, and 1st bending modes (Fig. 12). The 1st bending modes can also be observed as the most significant peak in the FAS of inclination data (Fig. 13). The sample FAS of acceleration data at 8:41 on July 9 are shown in Fig. 14. The tropical storm Elsa was sweeping through the area of BIWF on July 9, and the turbine was turned off and parked during this storm. It is observed that the second bending modes (2nd SS/FA) are evident in the FAS plot on July 9 which are around 2.0 Hz (2nd SS) and 2.3 Hz (2nd FA). However, only one peak at 2.3 Hz is present on April 22 when the turbine is in operation. Based on the system identification results presented in following sections, the 2nd FA/SS modes cannot be identified reliably using the data when the turbine is in operation but were identified with reasonable accuracy at parked/idling condition. The possible reason is that the 12P, as well as the second flapwise and edgewise modes of the blades have frequency close to the 2nd SS/FA modes, which causes modal interference and affects the system identification accuracy. The automatic system identification of the B2 wind turbine will be focused on the 1st FA/SS modes when the turbine is in operation, and both 1st and 2nd FA/SS modes at parked/idling conditions.

While the performance of the wired accelerometers has been exemplary, the wireless accelerometers did not provide reliable results. In particular, there were frequent losses of data (i.e. “drop-outs”) and it appeared that the battery life of the accelerometers was not consistent. It is hypothesized that the steel floors at each level hindered transmission of the wireless data to the Gateway, and more work is needed to find an optimal location for the Gateway.

3.2. Automatic system identification method

Modal parameters include natural frequencies, mode shapes and damping ratios which represent dynamic characteristics of structures. Modal parameters are informative structural signatures which are useful for condition assessment and response prediction [44]. In the recent years, modal parameters have been extensively used for structural assessment and response prediction. Model updating is one of the most common methods for the purpose of structural heath monitoring, and many applications of model updating have used modal parameters as data features to calibrate the numerical model and estimate uncertain parameters of the model [16–18,23,27].

Modal parameters can be identified using various types of dynamic measurements such as acceleration, velocity, strain, or displacement. Numerous system identification methods have been developed in the literature, including peak-picking [45], ARX method [46], general realization algorithm (GRA) [47], eigensystem realization algorithm (ERA) [48], ERA combined with the natural excitation technique (NExT-ERA) [49], frequency domain decomposition (FDD) [50], covariance-driven stochastic subspace identification (SSI–COV), and data-driven stochastic subspace identification (SSI-DATA) [51,52]. SSI-DATA is an output-only, parametric, and time-domain system identification method and is chosen and automated [53] for application in this project. SSI-DATA has been shown to provide accurate and unbiased results and is flexible for automation.

The acceleration measurements of B2 turbine were pre-processed and cleaned before they were fed into the SSI-DATA algorithm for extracting modal parameters. The spikes in the raw measurements were removed and replaced with interpolated values. The spikes were defined as any samples whose values were larger than 8 times the standard deviation of the signals. Then the cleaned signals were filtered between 0.1 and 3.2 Hz in frequency domain to focus on the frequency band of interest and remove the effect of high-frequency noise. The frequency band was selected to include the first few most important modes of the structure. The signals were finally down-sampled from 50 Hz to 8 Hz to improve the computation efficiency.

The basic idea of the SSI-DATA method is to fit a linear state-space model on output-only measurements under broadband excitation assumptions and provide estimates for the matrices **A** and **C** in the following state-space formulation of a stochastic linear dynamic system:

$$\begin{aligned} \boldsymbol{x}_{k+1} &= \boldsymbol{A}\boldsymbol{x}_k + \boldsymbol{w}_k \\ \boldsymbol{y}_k &= \boldsymbol{C}\boldsymbol{x}_k + \boldsymbol{v}_k \end{aligned} \tag{1}$$

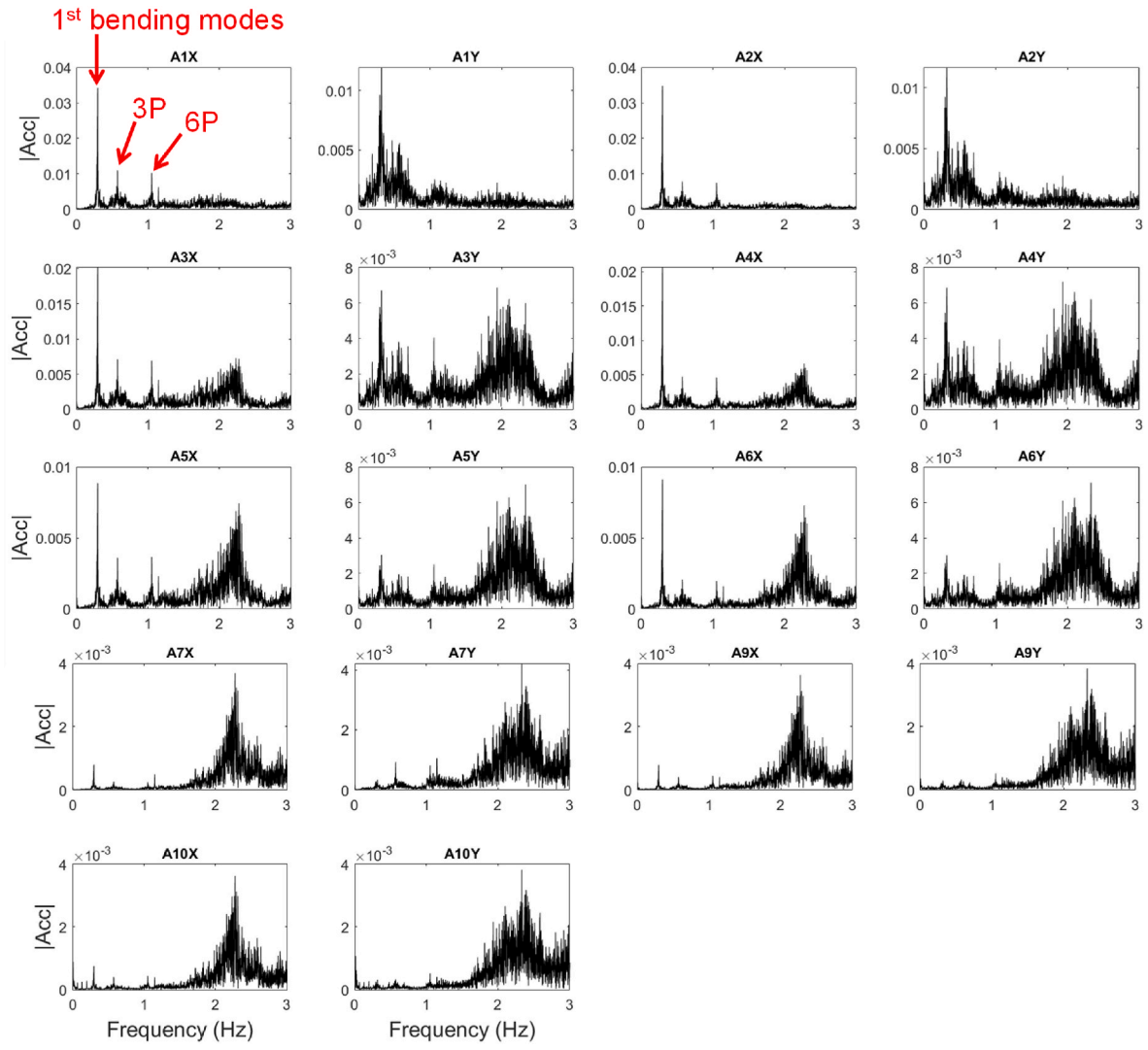

Fig. 11. Sample of FAS of acceleration at 9:17 on April 22.

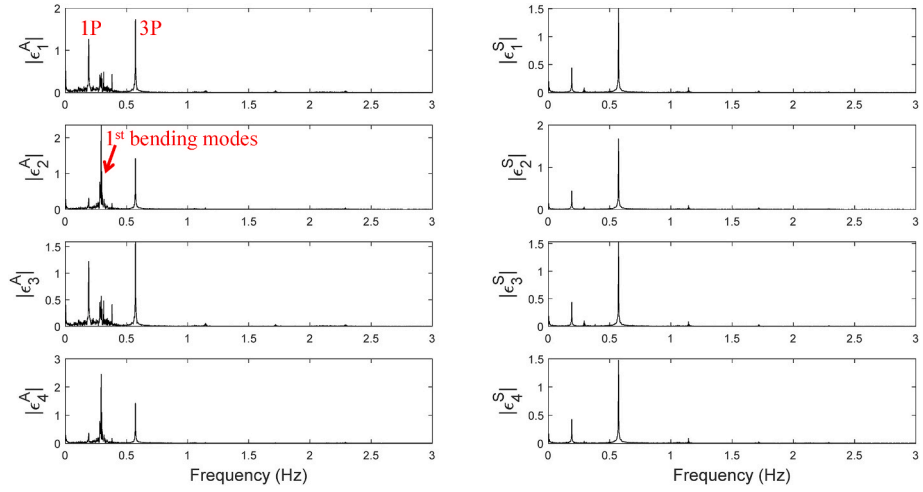

Fig. 12. Sample of FAS of strain at 16:03 on October 25.

where **x** is state vector, **A** is state matrix, **C** is output matrix, **y** consists of measurements, **w** and **v** denote input and output noise vector. The estimates of system matrices $\widehat{A}$ and $\widehat{C}$, involve creating Hankel matrices and singular value decomposition [46]. Then an eigenvalue analysis is performed on matrix $\widehat{A}$ as $\Lambda = \Psi^{-1}\widehat{A}\Psi$, where Λ is the eigenvalue matrix and Ψ is the eigenvector matrix. These system matrices are those of the

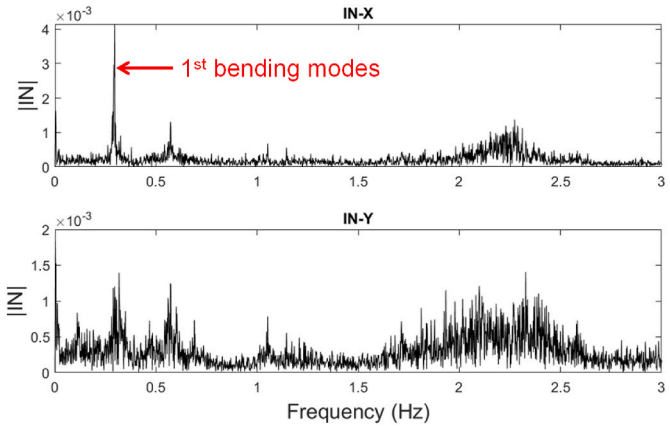

Fig. 13. Sample of FAS of inclination at 9:17 on April 22.

discrete system, and should be transformed into the original continuous time system, whose system matrix $\widehat{A}_c$ has the same eigenvector matrix as $\boldsymbol{\Psi}$, but its eigenvalue matrix is $\boldsymbol{\Lambda}_c = \frac{ln(\Lambda)}{\Delta t}$, where Δt is sampling time interval. The natural frequencies and damping ratios are computed as $\omega_i = \left|\lambda_{c,2i-1}\right|$, $\xi_i = -\frac{\text{Real}(\lambda_{c,2i-1})}{\omega}$, where $\lambda_{c,2i-1}$ is the diagonal component of eigenvalue matrix $\boldsymbol{\Lambda}_c$ and subscript '2*i*-1' means only odd eigenvalues are used because the eigenvalues are complex conjugate pairs and each pair provides modal parameters of one vibration mode. The mode shapes are estimated as $\boldsymbol{\Phi} = \widehat{\boldsymbol{C}}\boldsymbol{\Psi}$.

In the application of SSI-DATA for system identification, the system order (dimension of state matrix **A**) must be selected to fit a specific order of state space model to the measured data. If the measurement noise is zero and the system is observable, the system order can be simply determined as the number of nonzero singular values. However, for real-world applications, due to measurement noise and modeling errors, the division between significant and insignificant singular values is usually not obvious. If the selected system order is too small, then some vibration modes of interest may be missed. If the order is too high, then spurious modes will be included in the identified modal parameters. Therefore, a stabilization diagram is often utilized to select the appropriate order for the system and to detect the stable modes of interest. Stabilization diagram shows the evolution of modal parameters over different system orders, where physical modes are expected to have stable or similar modal parameters for different orders. Some limits or criteria can be chosen to judge if a mode is stable or not. The system order can be selected so the number of observable modes of interest is maximized, or alternatively, stable modes can be estimated using different orders for different modes. Modes which are not stable are treated as spurious modes and are excluded from modal identification results.

The automated system identification algorithm in this project is based on the following automation procedure: at each system order, the

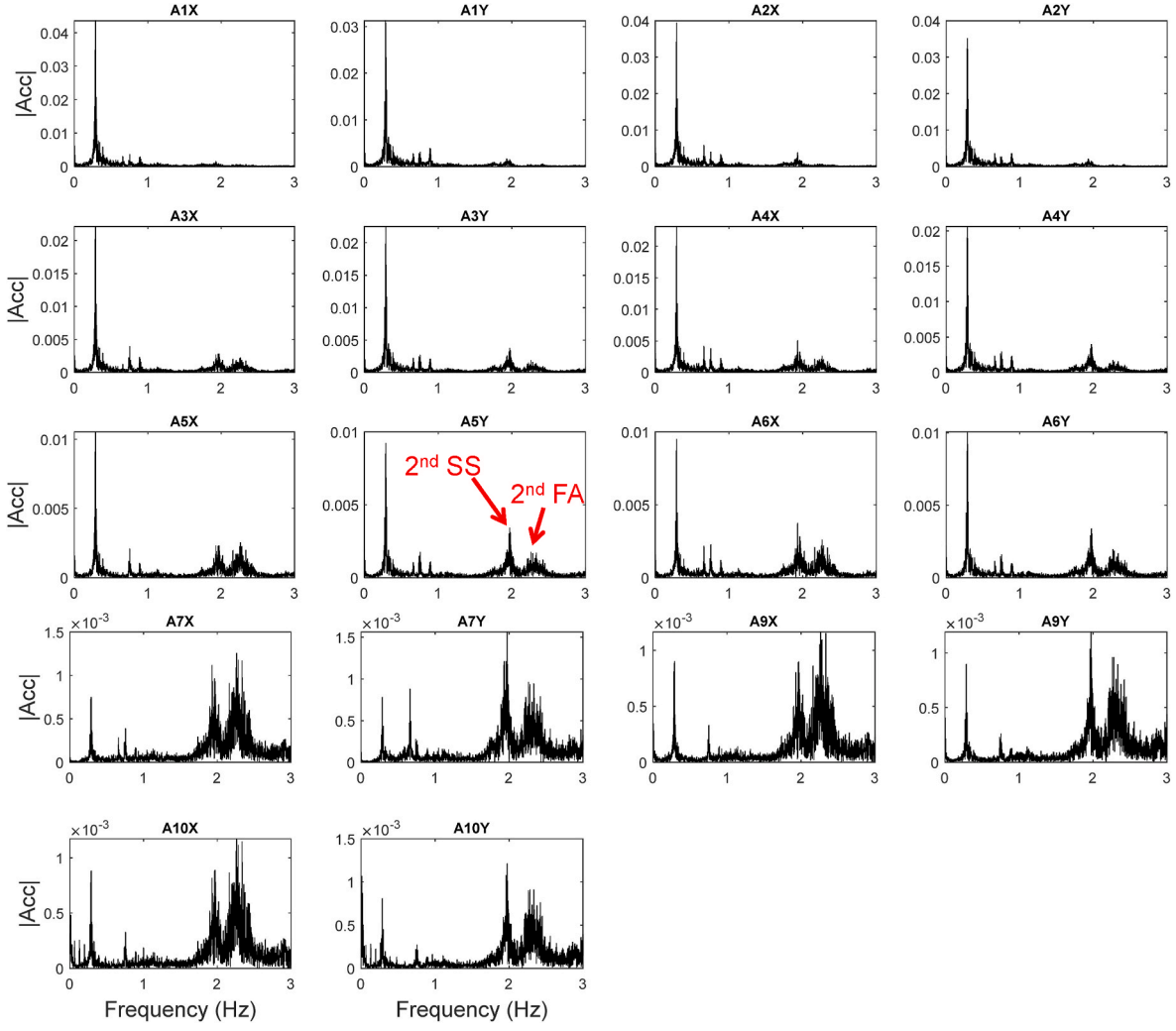

Fig. 14. Sample of FAS of acceleration at 8:41 on July 9 (parked turbine).

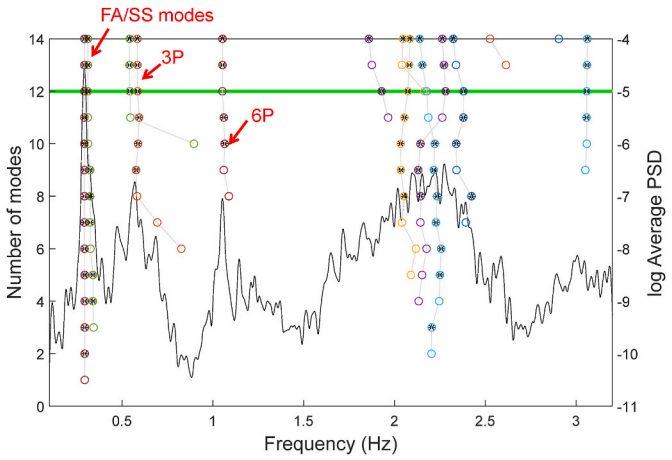

Fig. 15. Sample of frequency stabilization diagram at 9:17 on April 22.

identified modes are compared with their counterparts at previous order. If the relative difference of frequencies and damping ratios between current system order and previous order is less than a pre-selected threshold (2% for frequency and 50% for damping ratios) and the modal assurance criterion (MAC) value is larger than or equal to 0.9, then this mode is judged to be 'stable'. If a mode remains stable consecutively for 3 orders consecutively, then it is assumed to be a physical mode of the structure. Modes with unrealistic damping ratios, for example, less than zero or larger than 15%, will be excluded. Then the smallest order which provides a maximum number of physical modes of interest is selected as the best order of the state space model.

This study applies this automated system identification approach based on the SSI-DATA method to the unique monitoring data of the first commercial offshore wind farm in the U.S. with special jacket substructure and examines its performance under varying environmental and operational conditions over a period of one year.

3.3. System identification results

3.3.1. Identification of 1st FA/SS modes

The frequency stabilization diagram using the dataset at 9:17 on April 22 is shown in Fig. 15. The circles present potential modes, and starred circles refer to modes which satisfy the stability criterion for frequency, i.e., the relative difference of frequencies between successive orders is less than 2%. The horizontal green line denotes the final order of the state space model which is selected based on the aforementioned automation procedure. Note that the vertical ordinate here shows the number of modes, which is equal to half of the model order in state-

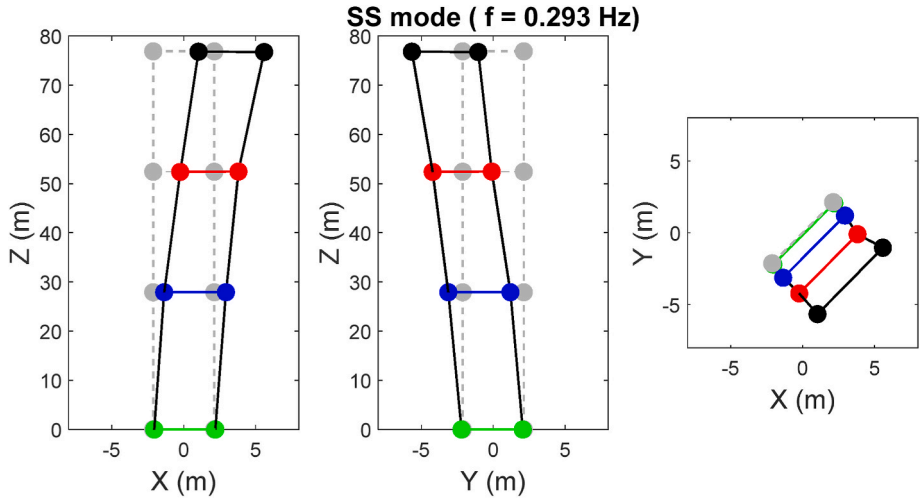

Fig. 16. Identified SS mode at 9:17, April 22.

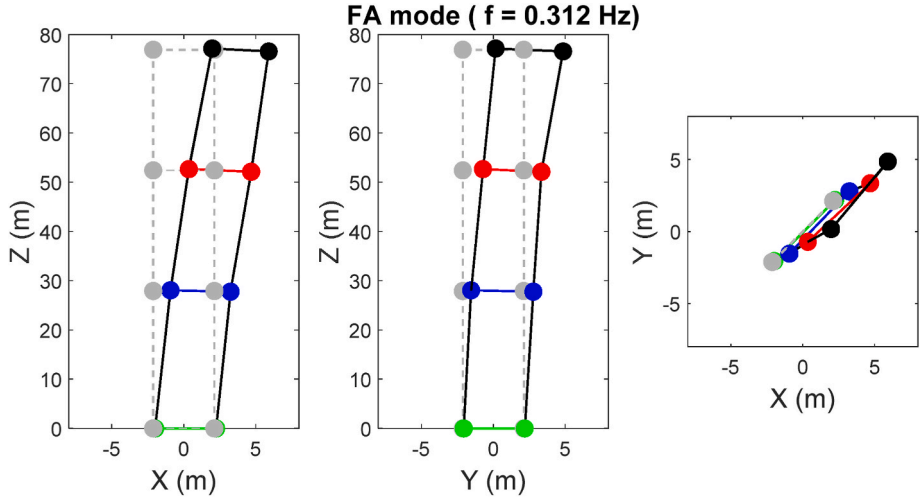

Fig. 17. Identified FA mode at 9:17, April 22.

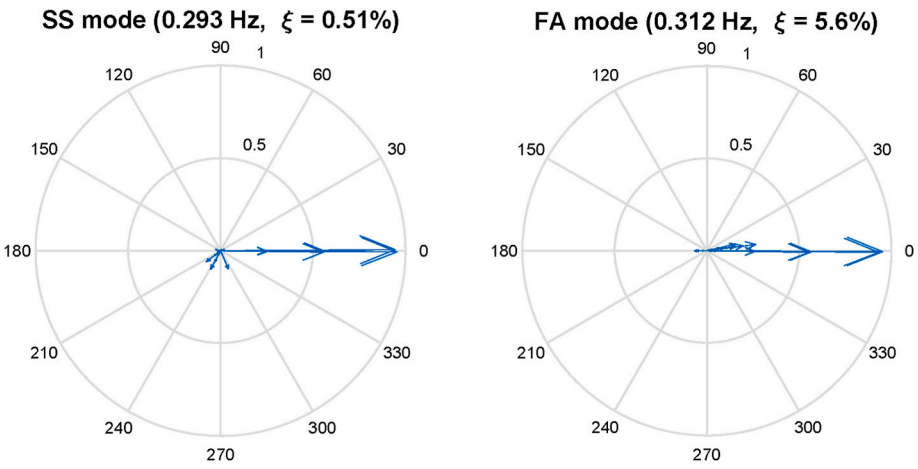

Fig. 18. Compass plot of identified SS/FA modes at 9:17, April 22.

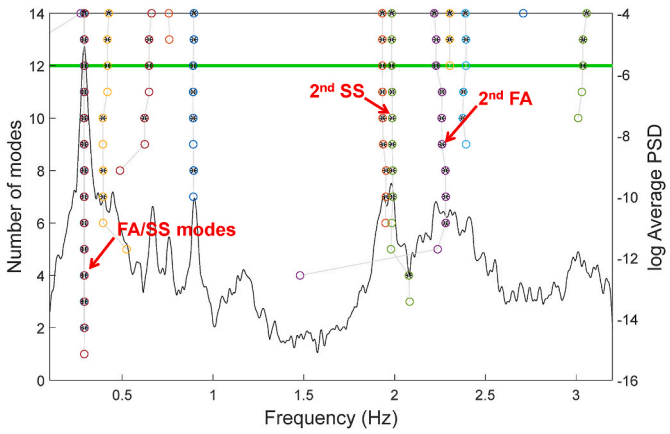

Fig. 19. Sample of frequency stabilization diagram at 8:31 on July 6.

space. The logarithm of averaged power spectral density (PSD) over all channels is also plotted in Fig. 15. It is observed that two closely-spaced modes are identified at around 0.3 Hz, which represent the FA and SS modes. In addition, 3P and 6P are also evident in the stabilization diagram. The mode shapes of SS and FA modes are shown in Figs. 16 and 17, respectively. Their compass plots representing the complex valued mode shapes (real vs. imaginary) are shown in Fig. 18. It is seen that the large components of FA and SS modes are almost collinear in complex plane, meaning that they are almost classically damped. It is also observed that since the FA/SS modes are closely-spaced, it is not possible to distinguish them based on just their frequencies. Therefore, mode shapes should be used to separate them, e.g., using modal assurance criteria (MAC). In this study, the FA and SS modes are separated by comparing them to the modal parameters from a reference dataset (i.e., 9:17 on April 22). Note that the mode shapes of FA/SS modes are affected by the yaw angle of the turbine, i.e., FA modes aligns with yaw angle while SS mode is perpendicular with yaw, therefore, the effects of yaw should be considered for more accurate separation of FA/SS modes. The detailed system identification results will be presented in a companion paper.

3.3.2. *Identification of 2nd FA/SS modes*

The 2nd FA/SS modes of the structure cannot be identified with reasonable accuracy when the turbine is in operation, probably due to the interference of the 2nd flapwise and edgewise modes of the blades, as well as the 12P, which have frequencies close to the 2nd FA/SS modes. Therefore, the data on July 6 was used to estimate the 2nd FA/SS modes using the same automated system identification process, because the turbine was parked on this day during the tropical storm Elsa. The frequency stabilization diagram at 8:31 on July 6 is shown in Fig. 19, where the 2nd SS and FA modes are present. It is seen that, unlike the results on April 22, the 2nd SS and FA modes can also be identified on

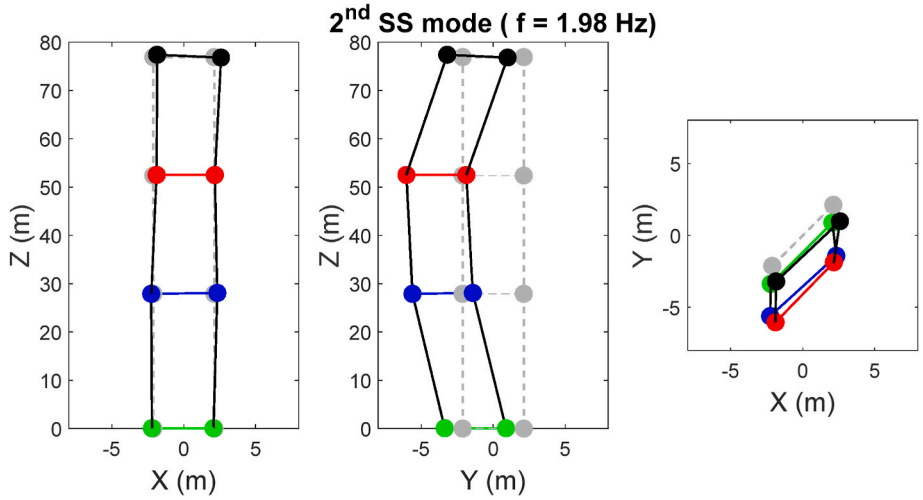

Fig. 20. Identified 2nd SS mode at 8:31 on July 6.

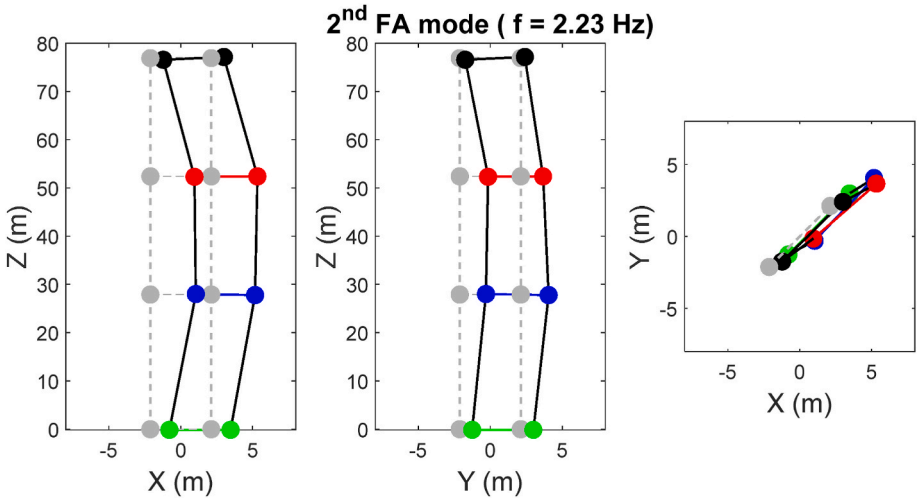

Fig. 21. Identified 2nd FA mode at 8:31 on July 6.

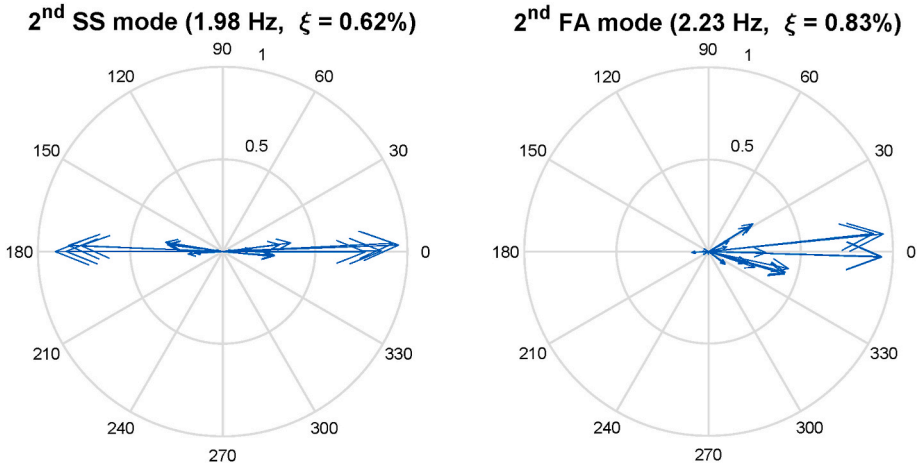

Fig. 22. Compass plot of 2nd SS/FA modes at 8:31 on July 6.

this day. The identified 2nd SS and FA mode shapes are shown in Figs. 20 and 21, respectively. The complex valued mode shapes are shown as compass plots in Fig. 22. It is seen that components of both 2nd SS/FA modes are almost collinear, meaning that they are classically damped. Because the frequencies of 2nd SS/FA modes are different (~2.0 Hz for 2nd SS mode and ~2.3 Hz for 2nd FA mode), they can be easily separated based on their frequencies.

4. Summary and conclusions

This study presents the installation details of the continuous monitoring system in the BIWF and investigates the applicability of the proposed automated system identification approach using the monitoring data, which has the following unique characteristics: (1) the monitoring data come from the first commercial offshore wind farm in the U.S.; (2) the monitoring system has been streaming data for more than a year and provides a landmark set of data for the purpose of prognosis and assessment of the utility-scale OWT; and (3) this monitoring system was specifically designed to be installed on an operational OWT for structural performance assessment and fatigue life prediction. The monitoring system includes wired and wireless accelerometers, SGs and inclinometer. The considerations for the instrumentation design are discussed, including the type, number and location of sensors. The DAQ, DEWEsoft-X3 for system configuration, and data transferring and storage are also introduced. A brief introduction of the automated system identification method using SSI-DATA is included. Samples of collected data are shown, and preliminary system identification results are presented. The FA/SS modes of the structure had been identified with high accuracy, and should be separated based on MAC values because their frequencies were closely-spaced. The 2nd FA/SS modes cannot be identified using the data when turbine was in operation due to the interference of 12P and modes of blades, but can be identified when turbine was parked or idling. The monitoring system has been continually collecting data and the automated system identification algorithm has provided estimated modal parameters of the structure over a year. The detailed system identification results under different operational conditions and over long period of time will be presented in a companion paper. These measurements and identified modal parameters serve as the database to represent the benchmark structural properties of the OWT for the purpose of structural health monitoring.

Declaration of competing interest

The authors declare the following financial interests/personal relationships which may be considered as potential competing interests: Eric Hines reports financial support was provided by U.S. Bureau of Safety and Environmental Enforcement (BSEE). Christopher Baxter reports financial support was provided by U.S. Bureau of Safety and Environmental Enforcement (BSEE). Mingming Song reports financial support was provided by U.S. Bureau of Safety and Environmental

Enforcement (BSEE). Per Sparrevik reports financial support was provided by U.S. Bureau of Safety and Environmental Enforcement (BSEE). Henrik Meland reports financial support was provided by U.S. Bureau of Safety and Environmental Enforcement (BSEE). James Strout reports financial support was provided by U.S. Bureau of Safety and Environmental Enforcement (BSEE). Aaron Bradshaw reports financial support was provided by U.S. Bureau of Safety and Environmental Enforcement (BSEE). Sau-Lon Hu reports financial support was provided by U.S. Bureau of Safety and Environmental Enforcement (BSEE). Babak Moaveni reports financial support was provided by U.S. Bureau of Safety and Environmental Enforcement (BSEE).

Per Sparrevik, Henrik Meland, and James Strout of NGI provide professional services for a number of OWT instrumentation systems in the North Sea as part of their regular business.

Jorge Basurto, was the contact at Ørsted during the initial monitoring campaign.

Dave Ciochetto was the project manager for the RI Coastal Resources Management Council.

We do not perceive these as conflicts of interest, but we are listing them for transparency.

Acknowledgements

This study has been completed as part of the Bureau of Safety and Environmental Enforcement (BSEE) project “Block Island wind farm structural monitoring project” under contract number 140E0119C0003. Additional support for this study has been provided by Massachusetts Clean Energy Center under the AmplifyMass program. The team is grateful to the help and support of GE Renewable Energy personnel including Trent Pack, Shane Watts, Jody Grainger, and Michael Hanson, as well as Ørsted personnel including Steven Wilkey, Bryan Wilson, Robert Gilpin, and Gavin Andrews for their help with installation of the monitoring system and access to the turbine SCADA data. The opinions, findings, and conclusions expressed in this paper are those of the authors and do not necessarily represent the views of the sponsors and organizations involved in this project.

References

[1] U.S. Energy Information Administration, https://www.eia.gov/(accessed 22 October 2022).
[2] W. Musial, P. Spitsen, P. Duffy, P. Beiter, M. Marquis, R. Hammond, M. Shields, Offshore Wind Market Report: 2022 Edition, U.S. Department of Energy, Office of Energy Efficiency and Renewable Energy., 2022. DOE/GO-102022-5765. August.
[3] Vestas V235-15.0 MW, https://www.vestas.com/en/products/offshore/V236-15MW/V236-15MW (accessed 22 October 2022).
[4] P. Tchakoua, R. Wamkeue, M. Ouhrouche, F. Slaoui-Hasnaoui, T.A. Tameghe, G. Ekemb, Wind turbine condition monitoring: state-of-the-art review, new trends, and future challenges, Energies 7 (4) (2014) 2595–2630.
[5] C. Dao, B. Kazemtabrizi, C. Crabtree, Wind turbine reliability data review and impacts on levelised cost of energy, Wind Energy 22 (12) (2019) 1848–1871.
[6] F.P.G. Márquez, A.M. Tobias, J.M.P. Pérez, M. Papaelias, Condition monitoring of wind turbines: techniques and methods, Renew. Energy 46 (2012) 169–178.
[7] Z. Hameed, Y. Hong, Y. Cho, S. Ahn, C. Song, Condition monitoring and fault detection of wind turbines and related algorithms: a review, Renew. Sustain. Energy Rev. 13 (1) (2009) 1–39.
[8] R. Rolfes, S. Tsiapoki, M. Häckell, Sensing solutions for assessing and monitoring wind turbines, in: Sensor Technologies for Civil Infrastructures, Elsevier, 2014, pp. 565–604.
[9] Z. Gao, X. Liu, An overview on fault diagnosis, prognosis and resilient control for wind turbine systems, Processes 9 (2) (2021) 300.
[10] C. Devriendt, F. Magalhães, W. Weijtjens, G. De Sitter, Á. Cunha, P. Guillaume, Structural health monitoring of offshore wind turbines using automated operational modal analysis, Struct. Health Monit. 13 (6) (2014) 644–659.
[11] G. Oliveira, F. Magalhaes, Á. Cunha, E. Caetano, Development and implementation of a continuous dynamic monitoring system in a wind turbine, Journal of Civil Structural Health Monitoring 6 (3) (2016) 343–353.
[12] CATAPULT, O. 7MW Levenmouth Demonstration Turbine. https://ore.catapult.org.uk/what-we-do/testing-validation/levenmouth/(accessed 22 October 2022).
[13] B. Moynihan, B. Moaveni, S. Liberatore, E. Hines, Estimation of blade forces in wind turbines using blade root strain measurements with OpenFAST verification, Renew. Energy 184 (2022) 662–676.
[14] FINO3, 2020. Available from: https://www.fino3.de/en/location/design.html.
[15] M. Song, S. Christensen, B. Moaveni, A. Brandt, E. Hines, Joint parameter-input estimation for virtual sensing on an offshore platform using output-only measurements, Mech. Syst. Signal Process. 170 (2022), 108814.
[16] Q. Zhang, T.-Y.P. Chang, C.C. Chang, Finite-element model updating for the Kap Shui Mun cable-stayed bridge, J. Bridge Eng. 6 (4) (2001) 285–293.
[17] J.M.W. Brownjohn, P. Moyo, P. Omenzetter, Y. Lu, Assessment of highway bridge upgrading by dynamic testing and finite-element model updating, J. Bridge Eng. 8 (3) (2003) 162–172.
[18] A. Teughels, G. De Roeck, Structural damage identification of the highway bridge Z24 by FE model updating, J. Sound Vib. 278 (3) (2004) 589–610.
[19] B. Jaishi, H.-J. Kim, M.K. Kim, W.-X. Ren, S.-H. Lee, Finite element model updating of concrete-filled steel tubular arch bridge under operational condition using modal flexibility, Mech. Syst. Signal Process. 21 (6) (2007) 2406–2426.
[20] E. Reynders, G.D. Roeck, P. Gundes Bakir, C. Sauvage, Damage identification on the Tilff Bridge by vibration monitoring using optical fiber strain sensors, J. Eng. Mech. 133 (2) (2007) 185–193.
[21] S.-E. Fang, R. Perera, G. De Roeck, Damage identification of a reinforced concrete frame by finite element model updating using damage parameterization, J. Sound Vib. 313 (3–5) (2008) 544–559.
[22] B. Moaveni, A. Stavridis, G. Lombaert, J.P. Conte, P.B. Shing, Finite-element model updating for assessment of progressive damage in a 3-story infilled RC frame, J. Struct. Eng. 139 (10) (2012) 1665–1674.
[23] M. Song, S. Yousefianmoghadam, M.-E. Mohammadi, B. Moaveni, A. Stavridis, R. L. Wood, An application of finite element model updating for damage assessment of a two-story reinforced concrete building and comparison with lidar, Struct. Health Monit. 17 (5) (2018) 1129–1150.
[24] J.L. Beck, L.S. Katafygiotis, Updating models and their uncertainties. I: Bayesian statistical framework, J. Eng. Mech. 124 (4) (1998) 455–461.
[25] K.-V. Yuen, Bayesian Methods for Structural Dynamics and Civil Engineering, John Wiley & Sons, 2010.
[26] E. Ntotsios, C. Papadimitriou, P. Panetsos, G. Karaiskos, K. Perros, P.C. Perdikaris, Bridge health monitoring system based on vibration measurements, Bull. Earthq. Eng. 7 (2) (2009) 469.
[27] H.-F. Lam, J. Yang, S.-K. Au, Bayesian model updating of a coupled-slab system using field test data utilizing an enhanced Markov chain Monte Carlo simulation algorithm, Eng. Struct. 102 (2015) 144–155.
[28] E. Simoen, G. De Roeck, G. Lombaert, Dealing with uncertainty in model updating for damage assessment: a review, Mech. Syst. Signal Process. 56 (2015) 123–149.
[29] M. Song, L. Renson, J.P. Noël, B. Moaveni, G. Kerschen, Bayesian Model Updating of Nonlinear Systems Using Nonlinear Normal Modes, Structural Control and Health Monitoring, 2018, p. e2258.
[30] G. Sevieri, M. Andreini, A. De Falco, H.G. Matthies, Concrete gravity dams model parameters updating using static measurements, Eng. Struct. 196 (2019), 109231.
[31] M. Song, B. Moaveni, C. Papadimitriou, A. Stavridis, Accounting for amplitude of excitation in model updating through a hierarchical Bayesian approach: application to a two-story reinforced concrete building, Mech. Syst. Signal Process. 123 (2019) 68–83.
[32] M. Song, R. Astroza, H. Ebrahimian, B. Moaveni, C. Papadimitriou, Adaptive Kalman filters for nonlinear finite element model updating, Mech. Syst. Signal Process. 143 (2020), 106837.
[33] E. Lourens, E. Reynders, G. De Roeck, G. Degrande, G. Lombaert, An augmented Kalman filter for force identification in structural dynamics, Mech. Syst. Signal Process. 27 (2012) 446–460.
[34] E. Zhang, J. Antoni, P. Feissel, Bayesian force reconstruction with an uncertain model, J. Sound Vib. 331 (4) (2012) 798–814.
[35] J. Sanchez, H. Benaroya, Review of force reconstruction techniques, J. Sound Vib. 333 (14) (2014) 2999–3018.
[36] S.E. Azam, E. Chatzi, C. Papadimitriou, A dual Kalman filter approach for state estimation via output-only acceleration measurements, Mech. Syst. Signal Process. 60 (2015) 866–886.
[37] F. Naets, J. Croes, W. Desmet, An online coupled state/input/parameter estimation approach for structural dynamics, Comput. Methods Appl. Mech. Eng. 283 (2015) 1167–1188.
[38] T. Pahn, R. Rolfes, J. Jonkman, Inverse load calculation procedure for offshore wind turbines and application to a 5-MW wind turbine support structure, Wind Energy 20 (7) (2017) 1171–1186.
[39] H. Ebrahimian, R. Astroza, J.P. Conte, C. Papadimitriou, Bayesian optimal estimation for output-only nonlinear system and damage identification of civil structures, Struct. Control Health Monit. 25 (4) (2018) e2128.
[40] M.S. Nabiyan, F. Khoshnoudian, B. Moaveni, H. Ebrahimian, Mechanics-based model updating for identification and virtual sensing of an offshore wind turbine using sparse measurements, Struct. Control Health Monit. 28 (2) (2021) e2647.
[41] M. Song, I. Behmanesh, B. Moaveni, C. Papadimitriou, Accounting for modeling errors and inherent structural variability through a hierarchical bayesian model updating approach: an overview, Sensors 20 (14) (2020) 3874.
[42] Ørsted, Ørsted Acquires Deepwater Wind and Creates Leading US Offshore Wind Platform, Company Announcement, 2018. https://orsted.com/en/company-announcement-list/2018/10/1819975. (Accessed 22 October 2022).
[43] C.R.M. Council, Block Island Wind Farm, 2015. http://www.crmc.ri.gov/windenergy/dwblockisland.html. (Accessed 22 October 2022).
[44] M. Friswell, J.E. Mottershead, Finite Element Model Updating in Structural Dynamics, vol. 38, Springer Science & Business Media, 2013.
[45] A.K. Chopra, A.K. Chopra, Dynamics of Structures: Theory and Applications to Earthquake Engineering, vol. 3, Pearson/Prentice Hall Upper, Saddle River, NJ, 2007.

[46] B. Peeters, System Identification and Damage Detection in Civil Engeneering, Katholieke Universiteit Leuven, 2000.
[47] R.A. De Callafon, B. Moaveni, J.P. Conte, X. He, E. Udd, General realization algorithm for modal identification of linear dynamic systems, J. Eng. Mech. 134 (9) (2008) 712–722.
[48] J.-N. Juang, R.S. Pappa, An eigensystem realization algorithm for modal parameter identification and model reduction, J. Guid. Control Dynam. 8 (5) (1985) 620–627.
[49] G. James, T.G. Carne, J.P. Lauffer, The natural excitation technique (NExT) for modal parameter extraction from operating structures, Modal Analysis-the International Journal of Analytical and Experimental Modal Analysis 10 (4) (1995) 260.
[50] R. Brincker, L. Zhang, P. Andersen, Modal identification from ambient responses using frequency domain decomposition, in: Proc. Of the 18th 'International Modal Analysis Conference, IMAC), San Antonio, Texas, 2000.
[51] P. Van Overschee, B. De Moor, Subspace Identification for Linear Systems: Theory—Implementation—Applications, Springer Science & Business Media, 2012.
[52] B. Peeters, G. De Roeck, Reference-based stochastic subspace identification for output-only modal analysis, Mech. Syst. Signal Process. 13 (6) (1999) 855–878.
[53] P. Moser, Continuous Monitoring of the Dowling Hall Footbridge, Tufts University, 2010.